Membrane Surface-Associated Helices Promote Lipid Interactions and Cellular Uptake of Human Calcitonin-Derived Cell Penetrating Peptides

Michael E. Herbig,* Kathrin Weller,* Ulrike Krauss,† Annette G. Beck-Sickinger,† Hans P. Merkle,* and Oliver Zerbe‡

*Drug Formulation and Delivery Group, Department of Chemistry and Applied BioSciences, Swiss Federal Institute of Technology Zurich (ETH Zurich), CH-8093 Zurich, Switzerland; †Institute of Biochemistry, University of Leipzig, D-04103 Leipzig, Germany; and ‡Institute of Organic Chemistry, University of Zurich, CH-8057 Zürich, Switzerland

ABSTRACT hCT(9-32) is a human calcitonin (hCT)-derived cell-penetrating peptide that has been shown to translocate the plasma membrane of mammalian cells. It has been suggested as a cellular carrier for drugs, green fluorescent protein, and plasmid DNA. Because of its temperature-dependent cellular translocation resulting in punctuated cytoplasmatic distribution, its uptake is likely to follow an endocytic pathway. To gain insight into the molecular orientation of hCT(9-32) when interacting with lipid models, and to learn more about its mode of action, various biophysical techniques from liposome partitioning to high-resolution NMR spectroscopy were utilized. Moreover, to establish the role of individual residues for the topology of its association with the lipid membrane, two mutants of hCT(9-32), i.e., W30-hCT(9-32) and A23-hCT(9-32), were also investigated. Although unstructured in aqueous solution, hCT(9-32) adopted two short helical stretches when bound to dodecylphosphocholine micelles, extending from Thr^{10} to Asn^{17} and from Gln^{24} to Val^{29}. A23-hCT(9-32), in which the helix-breaking Pro^{23} was replaced by Ala, displayed a continuous α-helix extending from residue 12 to 26. Probing with the spin label 5-doxylstearate revealed that association with dodecylphosphocholine micelles was such that the helix engaged in parallel orientation to the micelle surface. Moreover, the Gly to Trp exchange in W30-hCT(9-32) resulted in a more stable anchoring of the C-terminal segment close to the interface, as reflected by a twofold increase in the partition coefficient in liposomes. Interestingly, tighter binding to model membranes was associated with an increase in the in vitro uptake in human cervix epithelial andenocarcinoma cell line cells. Liposome leakage studies excluded pore formation, and the punctuated fluorescence pattern of internalized peptide indicated vesicular localization and, in conclusion, strongly suggested an endocytic pathway of translocation.

INTRODUCTION

Appropriate delivery of drugs to their sites of action is complicated by a number of factors. A prominent one is poor translocation through the cellular membrane that represents a major barrier for peptide, protein, and nucleic acid biopharmaceuticals. To aid in this process, several classes and/or prototypes of cell-penetrating peptides (CPPs) have been introduced during the past decade. Most of them consist of short, often oligocationic peptide sequences, which may be covalently linked to the compound of interest. Recently also, peptides capable of forming noncovalent complexes with the cargo have been developed (1–3).

The ability of CPPs to translocate the membrane when covalently linked or noncovalently complexed with a cargo renders them of broad interest in cell biology, biotechnology, and drug delivery. In fact, CPPs have been suggested as vectors for the cytoplasmic and nuclear delivery of hydrophilic biomolecules and drugs, both in vivo and in vitro (4–6). Initially, the mechanism of entry was firmly believed not to be mediated by receptors or transporters (4,5), suggesting a passive, nonendocytic transfer. However, it was soon recognized that cell fixation could cause artifactual uptake phenomena. Hence, the hypothesis of an energy-independent, direct transport of CPPs through biomembranes, as postulated in earlier CPP studies (7–9), had to give way to concepts involving endocytosis (10–14).

Much attention has been concentrated on the first step of CPP uptake, i.e., the interaction with the surface of the membrane leading to an enrichment and/or perturbation of the phospholipid bilayer, which may subsequently trigger endocytic uptake (14,15). In fact, in the few studies available in the literature that combine cell biological and biophysical approaches, good correlations between membrane affinity and uptake efficiency have been observed (16,17).

In this study, we determined the secondary structure and micellar localization of a human calcitonin-derived CPP, hCT (9-32), in contact with a membrane-mimicking environment, namely dodecylphosphocholine (DPC) micelles. Based on these results, we identified amino acids critical for membrane binding. Amino acids were replaced to enhance the affinity of the modified peptides toward biomembranes. The propensity of the modified peptides to bind to phospholipid bilayers was first assessed in liposome/buffer equilibrium dialysis experiments and compared to data for the wild-type peptide. A more detailed investigation of the positioning of the CPPs in DPC micelles was then performed in a NMR study utilizing a paramagnetic spin label. Finally the

Submitted June 14, 2005, and accepted for publication September 8, 2005.

Address reprint requests to Oliver Zerbe, Institute of Organic Chemistry, University of Zurich, Ch-8057 Zürich, Switzerland. Tel.: 41-44-63542 63; Fax: 41-44-6356833; E-mail address: oliver.zerbe@oci.unizh.ch.

0006-3495/05/12/4056/11 $2.00

doi: 10.1529/biophysj.105.068692

membrane translocating potential was investigated in a cell culture model.

Human calcitonin (hCT) is a peptide hormone that is approved for the treatment of established osteoporosis (18). N-terminally truncated derivatives of hCT, lacking hormonal activity, represent a novel class of weakly cationic CPPs and have been systematically investigated by Tréhin et al. (19). It has been shown that sequences from hCT(9-32) to hCT(18-32) could—at least to some extent—translocate the plasma membrane of a fully organized epithelial model, fully differentiated Madin-Darby canine kidney cell line (MDCK) monolayers, resulting in a sectoral, vesicular cytoplasmic distribution of the peptide. The uptake process was temperature, time, and concentration dependent, indicating that translocation may follow an endocytic pathway. Among the investigated derivatives hCT(9-32) was the most efficient one in this respect, and its single, positively charged lysine in position 18 turned out to be essential for uptake (19). Furthermore, uptake was found to be cell-line specific with a punctuated, cytoplasmic pattern in MDCK cells and paracellular accumulation in Calu-3 cell monolayers. Remarkably, hCT-derived peptides did not show significant permeation across epithelial models (20). This is owing to their efficient metabolic cleavage when in contact with epithelial cells (21).

In a previous ^{1}H NMR study, full-length hCT was structurally characterized in sodiumdodecylsulfate (SDS) micelles and found to form an amphipathic α-helix encompassing residues 9–6 (22). A recent solid-state NMR study showed that hCT(9-32) interacts preferably with the headgroups of a bilayer formed by a mixture of 1-palmitoyl-2-oleoyl-phosphatidylcholine (POPC), 1-palmitoyl-2-oleoyl-phosphatidylethanolamine (POPE), and 1-palmitoyl-2-oleoyl-phosphatidylglycerol (POPG) (in a 5:3:2 molar ratio) rather than with the hydrophobic core of the phospholipids (23). This work represents the first solution state NMR study to determine the secondary structure of hCT(9-32) and its orientation relative to the surface of the lipid micelle. As a result we observed formation of two short α-helical stretches in DPC micelles, which were interrupted by the Pro in position 23 for hCT(9-32). The wild-type sequence only moderately interacted with the interface of the micelles, whereas A23-hCT(9-32) revealed higher affinity for membrane binding due to its extended α-helix. Moreover, insertion of an additional, hydrophobic membrane anchor in W30-hCT(9-32) caused an even increased interaction with the micelle along the entire sequence. The enhanced affinity for membrane binding was reflected by a significantly higher uptake of W30-hCT(9-32) in human cervix epithelial andenocarcinoma cell line (HeLa) cells when compared to hCT(9-32).

MATERIALS AND METHODS

Deuterated docecylphosphatidylcholine (DPC-d_{38}, 99%-d) and dideuterium oxide (D_2O) were ordered from Cambridge Isotope Laboratories (Andover, MA). POPC of the best quality available was purchased from Avanti Polar Lipids (Alabaster, AL) and used without further purification. Melittin (purity >93%), 5-doxylstearic acid was bought from Aldrich (Buchs, Switzerland). The peptides used for uptake studies were N-terminally labeled with 5-carboxyfluoresein and synthesized by NMI Peptides (Reutlingen, Germany); their identity and purity (>95%) were controlled by mass spectral and high performance liquid chromatography (HPLC) analysis. Trifluoroacetic acid (TFA), manganese chloride (both analytical grade), calcein, acetic acid (reagent grade), phosphate-buffered saline (PBS) for buffer preparation, and Trypan blue solution in 0.81% sodium chloride and 0.06% potassium phosphate were purchased from Fluka (Buchs, Switzerland). hCT was kindly provided by Novartis Pharma AG (Basel, Switzerland).

Synthesis and purification of hCT-derived peptides

The sequences of the investigated hCT-derived peptides are given in Table 1. The peptides were synthesized by automated multiple solid phase peptide synthesis employing the Fmoc/tert. butyl strategy (24). After cleavage from the resin with TFA, the lyophilized peptides were purified by preparative reversed phase (RP) HPLC. The expected molecular weight was verified by matrix-assisted laser desorption/ionization-time of flight (MALDI-TOF) mass spectrometry (Voyager Perseptive II, Weiterstadt, Germany), and retention times were determined using a LiChrospher 100 RP-18 column with a linear gradient mobile phase starting at 90% solvent A (water/TFA, 99.9:0.1) (v/v) and 10% solvent B (acetonitrile/TFA, 99.92:0.08) (v/v) to 60% solvent B over 30 min at a flow rate of 1 mL/min: A23-hCT(9-32): $mass_{calc.}$ 2583.8 Da, $mass_{exp.}$ 2584.90 Da, RP-HPLC retention time 19.41 min; W30-hCT(9-32): $mass_{calc.}$ 2739.0 Da, $mass_{exp.}$ 2740.72 Da, HPLC retention time 20.75 min.

Preparation of LUVs

Large unilamellar vesicles (LUVs) were prepared by dissolving the phospholipids in chloroform to ensure complete solution and mixing of the components. The lipids were dried at 37°C in a rotary evaporator to yield a thin film and then kept under high vacuum over night. The dry film then was redispersed in the buffer and the resulting multilamellar vesicle (MLV) dispersion was subjected to five freeze-thaw cycles. LUVs were obtained by extruding four times through 0.4 μm and eight times through 0.1 μm Nuclepore polycarbonate membranes. Lipid concentration was determined

TABLE 1 Abbreviations, amino acid sequences, and molecular weights of the peptides studied in this work; amino acid substitutions are underlined

Abbreviation	MW (Da)	Sequence
hCT	3417.8	CGNLS TCMLG TYTQD FNKFH TFPQT AIGVG AP-NH_2
hCT(9-32)	2609.9	LG TYTQD FNKFH TFPQT AIGVG AP-NH_2
A23-hCT(9-32)	2583.8	LG TYTQD FNKFH TF<u>A</u>QT AIGVG AP-NH_2
W30-hCT(9-32)	2739.0	LG TYTQD FNKFH TFPQT AIGV<u>W</u> AP-NH_2
hCT-random	2609.9	FL TAGQN TIQTP VKTGG HFPFA DY-NH_2

by an enzymatic colorimetric test for phospholipids (MPR 2) obtained from Roche Diagnostics (Mannheim, Germany), and the LUV size was checked by photon correlation spectroscopy on a Zetasizer 3000 HSA (Malvern, UK).

Liposome-buffer partitioning experiments

Liposome-buffer partitioning experiments were performed by equilibrium dialysis through a cellulose dialysis membrane, molecular weight cutoff 10,000 Da, at 37°C during 7 h using a protocol described by Pauletti et al. in more detail (25). Lipid concentrations of 4 mM and peptide concentrations of 20 μM were used. For HPLC analysis, liposomes were dissolved in a threefold excess of methanol and analyzed according to the method described by Buck and Maxl (26). In all measurements, values at 7 h were used for calculation of apparent partition coefficients (D) according to Schurtenberger et al. (27):

$$D = \frac{C_{P(b)}}{C_{P(f)} \times C_L}, \quad (1)$$

where $C_{P(b)}$ is the concentration of peptide bound to liposomes, $C_{P(f)}$ the concentration of free peptide, and C_L is the concentration of lipid molecules. $C_{P(b)}$ was calculated by subtracting the peptide concentration in the buffer compartment from the peptide concentration in the liposome compartment.

Preparation of calcein-containing LUVs

LUVs were prepared by dissolving the phospholipids in chloroform as described above. The lipids were dried at 37°C in a rotary evaporator to yield a thin film and then kept under high vacuum over night. The dry film then was redispersed in buffer (20 mM calcein, in PBS pH 7.4, containing 1 mM EDTA for complexing of Ca^{2+}/Mg^{2+}, which could affect calcein fluorescence), and the resulting MLV solution was treated by five freeze-thaw cycles. LUVs were then obtained by extruding four times through 0.4 μm and eight times through 0.1 μm Nuclepore polycarbonate membranes (28). A plastic syringe mounted in a centrifugation tube was filled with hydrated Sephadex G-50 gel. Untrapped dye was removed by the minicolumn centrifugation method (29) by spinning at 200 g for 3 min.

Dye efflux measurements

A total of 50 μL of a 400 μM LUV suspension was injected into 96 well plates (Nunc, Wiesbaden, Germany) containing 50 μL of peptide solutions of different concentration. Calcein leakage from vesicles was monitored fluorimetrically by measuring the decrease in self-quenching (excitation at 462 nm, emission at 525 nm) after 60 min at room temperature on a Varian Cary Eclipse spectrofluorometer (Mulgrave, Australia). The buffer blank was subtracted form all values, and the fluorescence intensity corresponding to 100% leakage was determined after the addition of Triton X-100 (30). Results were displayed as percentage of maximum leakage.

NMR spectroscopy

Accelerated exchange of amide protons in smaller peptides limits the use of this technique to values between ~3 and 5, whereas the apparent pH in the water-micelle interface is lightly shifted, allowing us to record data at higher pH. Moreover, line widths of micelle-associated peptides are larger due to the increased time for rotational diffusion (39). Therefore, experimental conditions were adjusted to meet the specific requirements in these two environments. Accordingly, all NMR experiments utilized 2 mM solutions of peptides at pH 5.6 in the presence of 300 mM d_{38}-dodecylphophocholine (resulting in ~1 peptide associated to every third micelle (31)) in 90% H_2O/D_2O, and spectra were recorded at 310 K on a Bruker (Karlsruhe, Germany) DRX-500 spectrometer. In our investigations of the peptides in the absence of detergent, data were recorded at pH 4.1 and at 300 K. Sequence-specific resonance assignments were performed based on two-dimensional data from 12 ms and 40 ms clean total correlation NMR spectroscopy (TOCSY) experiments (32) and from a 120 ms nuclear Overhauser effect NMR spectroscopy (NOESY) experiment (33). Otherwise, we largely followed protocols developed by Wüthrich and co-workers for assignment purposes (34). Upper limits derived from the NOESY data were used as restraints for torsion angle molecular dynamics runs performed within the program DYANA (35), using its standard simulated annealing protocol.

To determine the micelle-binding interface, we measured the decrease in peak intensity in the 12 ms TOCSY spectra after addition of the micelle-integrating spin label 5-doxylstearate, which was previously shown to be positioned in vicinity to the phospholipids' headgroups (36,37). We computed two subsets of values corresponding to integrals from only the H^N,H^α crosspeaks in the fingerprint region and from the average from all peaks corresponding to one amino acid and analyzed their intensity ratio in the presence and absence of the spin labels as determined in the program XEASY (38). Otherwise we used methodology described by us in more detail in Bader et al. (39,40).

Cell culture

HeLa cells, a human cervix epithelial adenocarcinoma-derived cell line, used throughout this study, were obtained from American Type Culture Collection ATCC (Rockville, MD). Cells were used within five passages. Cell culture was maintained under standard cell culture conditions in humidified 5% CO_2. Cells were cultured as exponentially growing subconfluent monolayers and maintained in Dulbecco's modified Eagles medium with GlutaMAX, sodium pyruvate, 4500 mg/L glucose, supplemented with 10% heat-inactivated fetal calf serum and penicillin/streptomycin (100 units/mL and 100 μg/mL, respectively).

Confocal laser scanning microscopy—uptake studies in living cells

To assess the cellular localization of the investigated fluorescent labeled CPPs, we performed confocal laser scanning microscopy (CLSM). Exponentially growing HeLa cells were seeded onto eight well Lab-Tek chambered coverglasses at a density of 35,000 cells/cm^2. Cells were used 1 day after seeding. For uptake experiments, cells were incubated for 2 h in serum-free medium containing fluorescence-labeled CPP or unconjugated 5-carboxyfluorescein (Fluka) as a control at a concentration of 40 μM. A total of 4 mM stock solutions of the CPP or of unconjugated carboxyfluorescein were prepared in DMSO to increase the solubility and subsequently diluted (1:100) with serum-free medium to a final concentration of 40 μM. This concentration was chosen in agreement with previous studies (19,20), as the uptake mechanism of hCT-derived peptides may involve enrichment (41) and self-assembly (42) of peptide in the membrane interface. The concentration of DMSO was 1%. Simultaneously, nuclei were stained with 1 μg/ml Hoechst 33342 (Molecular Probes, Leiden, The Netherlands) for 30 min. Subsequently, cells were rinsed three times with Hanks' balanced salt solution buffer (HBSS) and overlaid with HBSS buffer for observation using CLSM. To avoid misinterpretation due to unspecifically bound extracellular fluorescence, one-half of the volume was replaced with an aqueous 0.4% Trypan blue solution to quench extracellular fluorescence (43–45). Cells were then scanned using a Zeiss (Jena, Germany) CLSM 410 inverted microscope. Image processing was performed using Imaris (Bitplane, Zurich, Switzerland).

Fluorescence-activated cell sorting—quantification of internalized CPP

To quantify internalized fluorescence-labeled CPP, we performed a fluorescence-activated cell sorting analysis (FACS). Again, exponentially growing

HeLa cells were seeded onto 24 well plates at a density of 35,000 cells/cm^2 and were used 1 day after seeding. For uptake experiments, cells were incubated for 2 h in serum-free medium containing fluorescence-labeled CPPs or unconjugated 5-carboxyfluorescein as a control at a concentration of 40 μM. A total of 40 μM solutions of the CPPs or of unconjugated dye was prepared analogously to the procedure used in the CLSM. After incubation, all cells were extensively washed with PBS buffer, and cells were treated with trypsin for 7 min to detach cells from the surface and to digest membrane-bound peptide as adopted from the literature (13,46) and washed once more with PBS before measurement. After addition of Trypan blue as a quencher for extracellularly bound fluorescence (47,48), FACS was performed on a FacScan (BectonDickinson, Franklin Lakes, NJ) within 1 h after trypsinization. A total of 8000 gated cells per sample were analyzed using Cytomation Summit software (Cytomation, Fort Collins, CO). The 5-carboxyfluorescein control value was subtracted, and results were normalized to the unmodified hCT(9-32). Statistical comparisons for significance were made with Student's t-test; $p \leq 0.02$ was considered statistically significant. All experiments were performed in triplicate.

To check for cell proliferation and viability of HeLa cells after 1 h of incubation with the so-far not tested CPP A23-hCT(9-32) and W30-hCT(9-32), we measured the overall activity of mitochondrial dehydrogenase (MTT assay) according to the instructions of ATCC (ATCC, MTT Cell Proliferation Assay Instructions) (49). Briefly, HeLa cells were incubated in 96 well plates (Nunc, Roskilde, Denmark) to 70–80% confluency and then incubated as described above. As controls we used untreated cells and cells treated with methanol for 7 min, respectively. After discarding the CPP solutions, MTT (Sigma, St. Louis, MO) was added for 4 h at 37°C. After removing the MTT solution, the purple precipitate was dissolved for 12 h by addition of detergent (81 ml isopropanol, 15 ml SDS 20%, 4 ml 1 M HCl). Overall activity of MTT in each well was measured spectrophotometrically at 570 nm using a ThermoMax microplate reader (Molecular Devices, Sunnyvale, CA).

RESULTS

Liposome-buffer partitioning experiments

To test the propensity of hCT to interact with cell membranes, partition coefficients were determined in a liposome-buffer equilibrium system (25). In contrast to partitioning studies in isotropic media, e.g., water/octanol, anisotropic media like liposomes also include ionic interactions and, therefore, represent a more realistic model. All LUV liposomes prepared displayed unimodal size distributions with mean diameters of 103.4 $\pm$ 1.9 nm for POPC. A large lipid/peptide molar ratio ($\sim$200) was chosen to establish a biologically relevant lipid/peptide ratio and to exclude formation of specific lipid-peptide aggregates.

Since our NMR studies revealed that at least some of the peptides (e.g., A23) form aggregates at neutral pH, a pH of 3.5 was chosen to avoid problems associated with differential aggregation. The apparent partition coefficients D at that pH were determined after 7 h. Fig. 1 demonstrates the resulting partition coefficients of various hCT-derived CPPs in neutral POPC LUVs. For hCT(9-32) a D of 66 was determined; it increased by a factor of 2 when replacing Gly^2 or Gly^{30} by Trp. Among all amino acids, Trp is known to partition most into the water-membrane interface (50). Also the replacement of the helix-breaking Pro^{23} by Ala, bridging the two short α-helical segments, caused a 1.7-fold increase in D. The hCT(9-32) derivative with a randomized amino acid sequence showed a largely reduced D value as compared to hCT(9-32), indicating that not only the amino acid composition but also the secondary structure and possibly the amphipathicity played a significant role for the affinity toward membranes.

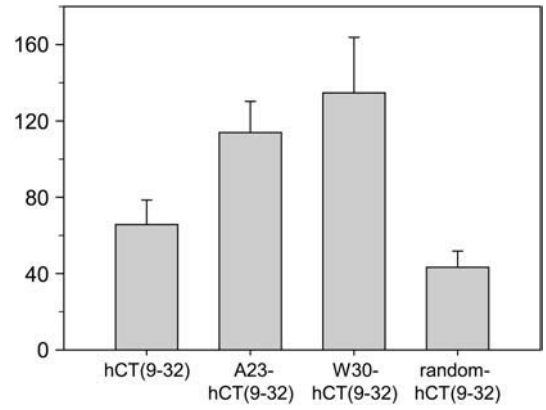

FIGURE 1 Apparent liposome-buffer partitioning coefficients between extruded POPC LUVs and acetic acid/acetate buffer, pH = 3.5, at a total lipid concentration of 4 mM and a peptide concentration of 20 μM. Dialysis was performed for 7 h at 37°C. Results are represented as mean $\pm$ SD of three independent experiments.

Peptide effects on bilayer integrity: calcein leakage experiments

An advantage of hCT-derived CPPs is their low toxicity: hCT is a human hormone and an approved drug for the treatment of postmenopausal osteoporosis (18). Furthermore, Tréhin et al. (20), using several cell lines, demonstrated the absence of cytotoxic effects of hCT(9-32), even when incubated for periods as long as 24 h. To investigate whether the amino acid substitutions in A23-hCT(9-32) and W30-hCT(9-32) increased their potential to affect the integrity of phospholipid membranes, we performed a dye leakage assay with calcein-loaded POPC LUVs. As shown in Fig. 2 we compared membrane-permeabilizing effects at increasing concentrations of the hCT-derived CPPs and melittin as control in a 200 μM suspension of neutral POPC LUVs at pH 7.4. Melittin is a basic, amphipathic 26-amino acid peptide for which pore formation in lipid bilayers has been previously demonstrated to lead to complete calcein leakage at peptide concentrations as low as 1 μM (51). In contrast, hCT caused a leakage of only $\sim$8% at a peptide concentration of 40 μM, which corresponds to a peptide/lipid ratio of 0.2. None of its derivatives exhibited any significant leakage. At the highest concentration of 200 μM, corresponding to a peptide/lipid ratio of 1.0, hCT caused a leakage of $\sim$40%. The values for A23-hCT(9-32) and W30-hCT(9-32) were markedly lower, and hCT(9-32) caused a leakage of $\sim$10% only.

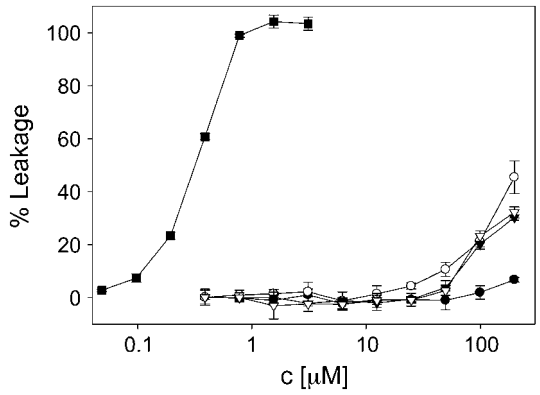

FIGURE 2 Percentage leakage of the LUV-entrapped fluorescent dye calcein as a function of peptide concentration. Peptide solutions up to a final concentration of 200 μM were added to a 400 μM POPC LUV solution in PBS buffer, pH 7.4. From the increase of calcein fluorescence, the peptide-induced leakage in percentage was calculated for melittin (■), hCT (○), hCT(9-32) (●), A23-hCT(9-32) (△), and W30-hCT(9-32) (▲). Data were recorded after 60 min of incubation at ambient temperature (~22°C) and are represented as mean ± SD ($n = 3$).

Structural data from NMR experiments

200 ms NOESY data of hCT(9-32) in pure aqueous solution at pH 4.1 indicates that the peptide is unstructured in solution. The NOESY spectra are devoid of medium range contacts and only display intraresidual and sequential nuclear Overhauser effects (NOEs). This observation is supported by scalar coupling constants close to rotationally averaged values of ~7 Hz.

We also recorded a 120 ms NOESY on hCT(9-32) in the presence of DPC micelles. Continuous stretches of sequential NOEs of amide protons ($H^N(i),H^N(i + 1)$) were observed between Thr^{10}–Ans^{17} and Gln^{24}–Val^{29}. In addition, a few H^α,H^N ($i,i + 2$) and $H^\alpha,H^\beta(i,i + 3)$ restraints were also observed in these stretches. Structure calculations within the program DYANA confirmed helical folds in these segments. However, the polypeptide conformation was not sufficiently well defined to assign the conformation to a specific helix type, and the data clearly indicated that residual flexibility was contained in the structures (e.g., scalar couplings $^3J(H^N,H^\alpha)$ adopted values between 6 and 7 Hz). As derived from the structure calculations, hCT(9-32) forms two amphipathic helices connected via a flexible linker, which is terminated by Pro^{23}.

We used the micelle-integrating spin labels 5- and 16-doxylstearate to probe the orientation of the peptide on the micelle. Whereas the former spin label probes vicinity to phospholipid headgroups, the latter should affect protons more deeply inserted into the micelles. We also added Mn^{2+} to the micellar solution, a spin label that mostly affects solvent-exposed protons. The relative signal attenuation due to the presence of 5-doxyl stearate was plotted against the sequence of each of the three peptides hCT(9-32), A23-hCT(9-32), and W30-hCT(9-32). Signal attenuations for all three peptides largely followed periodic patterns. Interestingly, the amount of signal reductions generally followed the order of hCT(9-32) < A23-hCT(9-32) < W30-hCT(9-32), indicating that the micellar association of the Trp^{30} analog was tighter than for the other two peptides. Moreover, introduction of Trp at position 30 induced membrane association of the C-terminal tetrapeptide. Helical periodicity was most clearly observed for A23-hCT(9-32). Prominent signal reductions were mainly observed for the aromatic amino acids Tyr^{12}, Phe^{16}, 19 and 22 as well as for His^{20}, and for Ala^{23} and Gly^{28}. Our observations are fully compatible with thermodynamic data of partitioning whole amino acids into water-membrane interfaces as measured by White and Wimley (50). We noticed that only weak signal reductions were observed in the C-terminal half of hCT(9-32). To investigate whether the C-terminus integrated into the micelle interior or was freely diffusing in solution, we conducted experiments with the spin label Mn^{2+}. As a result we observed significant signal reductions for the C-terminal segment of hCT(9-32) (see Fig. 3 *D*), proving that this part protruded into the aqueous phase. However, we also observed signal reductions in the region around residue 15 (data not shown), indicating that Mn^{2+} also coordinated to the side-chain carboxy group of Asp^{15}. The replacement of Pro^{23} by Ala resulted in the extension of the amphipathic helix, but whether this structural effect or the more favorable partitioning properties of Ala when compared to Pro led to higher uptake is presently unclear. Nevertheless, Trp^{30} introduced a new membrane anchor in the C-terminal tetrapeptide domain, resulting in stronger and more homogenous signal reductions along the sequence. As derived from these spin label studies, the membrane-binding affinities followed the order of hCT(9-32) < A23-hCT(9-32) < W30-hCT(9-32). This result is most likely due to the extent to which the C-terminal part of the peptides associated with the micelle. Patterns for signal reductions due to the spin label 16-doxylstearate were similar in their trend but less pronounced, excluding that the peptides more deeply penetrate the micelle interior.

Confocal laser scanning microscopy: uptake studies in living cells

Recently, an intense debate occurred in the literature whether artifacts in the mechanistic interpretation of CPP studies were caused through cell fixation. Even mild fixation protocols have been described to give rise to misleading interpretations about peptide internalization. Therefore, throughout, we conducted our cellular uptake study in living, nonfixed HeLa cells. In addition, we were aware that routine washings with buffer did not reliably remove all membrane-bound CPP as already found in previous studies (13). For both CLSM and FACS we quenched extracellular fluorescence using Trypan blue. Cells were exposed to either one of the three CPP or the

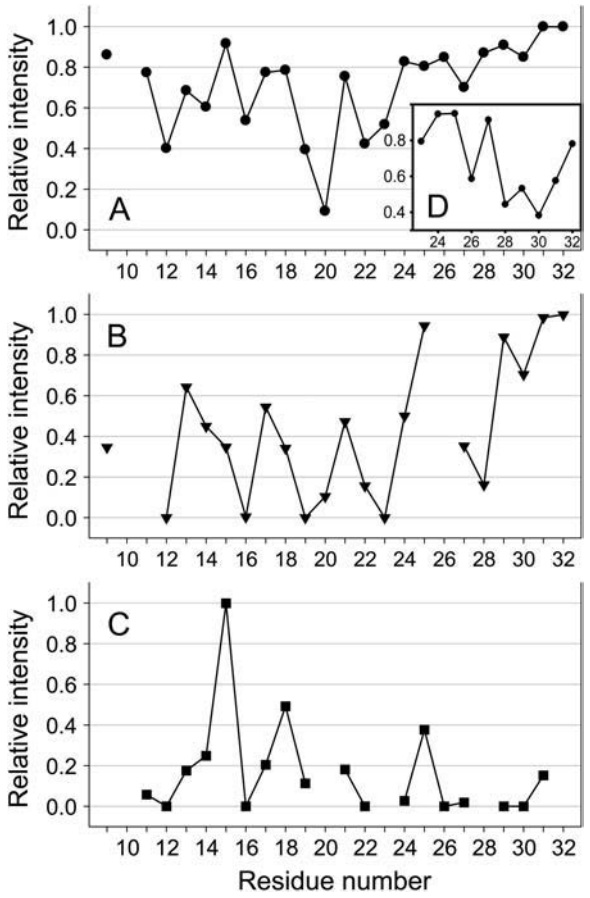

FIGURE 3 Relative signal intensities in ^{1}H-TOCSY spectra of hCT-derived peptides in DPC micelles in presence of the spin label 5-doxylstearic acid with respect to a reference spectrum without spin label. 2 mM solutions of hCT(9-32) (*A*), A23-hCT(9-32) (*B*), and W30- hCT(9-32) (*C*) were measured in 300 mM d_{38}-DPC micelles at pH 5.6. The inset in *A* depicts the reduction for hCT(9-32) in the presence of the spin label manganese chloride with respect to a reference spectrum without spin label (*D*).

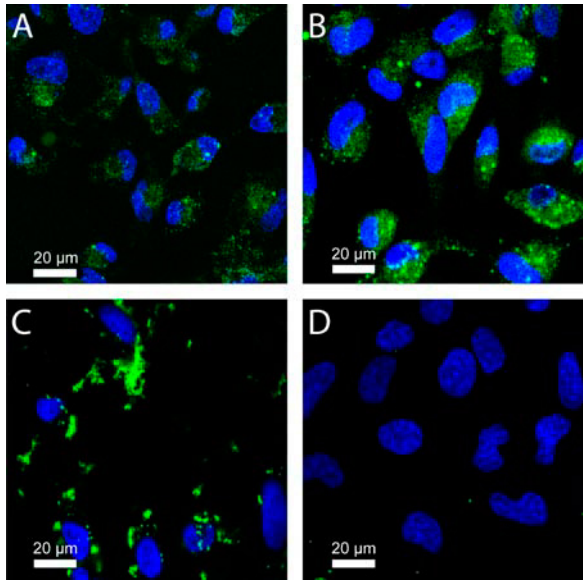

FIGURE 4 Confocal microscopy of translocation of hCT(9-32) and its modifications in HeLa cells. HeLa cells were incubated for 2 h with 40 μM peptide solution in serum-free medium of (*A*) hCT(9-32), (*B*) W30-hCT (9-32), (*C*) A23-hCT(9-32), or (*D*) 5-carboxyfluorescein. Cell nuclei (in *blue*) were stained for 30 min with Hoechst 33342 at a concentration of 1 μg/ml. For extracellular fluorescence quenching, CLSM pictures were taken after addition of Trypan blue.

Quantitative assessment of peptide internalization by FACS analysis

In addition to the general trends in translocation as observed by CLSM, cellular uptake of the CPPs was also monitored through FACS analysis. HeLa cells were incubated for 2 h with either the respective CPP or 5-carboxyfluorescein as control at concentrations of 40 μM. The relative median

unconjugated dye. After incubation at 37°C for 2 h, cells showed cellular uptake of all investigated peptides. Cell nuclei were stained with Hoechst 33342. hCT(9-32) (Fig. 4 *A*) and W30-hCT(9-32) (Fig. 4 *B*) exhibited punctuated fluorescence patterns indicating that the translocated fluorescence was localized in discrete vesicular compartments in the cytoplasm, suggestive of an endocytic pathway of internalization.

The cytosolic fluorescence of W30-hCT(9-32) was higher as compared to the unmodified hCT(9-32), indicating a more efficient uptake. The coarse fluorescence pattern for A23-hCT(9-32) (Fig. 4 *C*) suggests that, owing to its limited solubility in serum-free medium, the peptide may have aggregated in larger clusters on the cell membrane, which cannot be completely quenched by Trypan blue. No intracellular fluorescence was observed in control cells incubated with the fluorescence marker 5-carboxyfluorescein alone (Fig. 4 *D*).

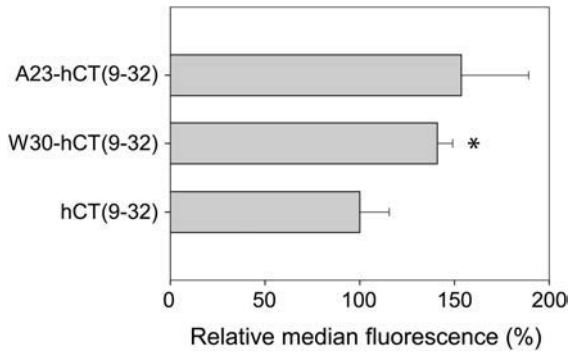

FIGURE 5 Quantification of cellular internalization of hCT(9-32) and its modifications in HeLa cells. HeLa cells were incubated with 40 μM peptide solutions in serum-free medium for 2 h. FACS analysis was performed after the addition of Trypan blue to quench extracellular fluorescence. The internalization of the unmodified hCT(9-32) was set to 100%, the modifications' internalization efficiency are expressed as relative percentages. The results are represented as mean ± SD ($n = 3$). Asterisk indicates a statistically significant difference ($p < 0.02$).

fluorescence of the cells after internalization is demonstrated in Fig. 5. Again, Trypan blue was added as a quencher for extracellularly bound fluorescence. For A23-hCT(9-32) a more extensive membrane binding was observed as compared to the other two CPP as shown by a more pronounced reduction in fluorescence after incubation with the quencher (data not shown). The relative median fluorescence of HeLa cells after uptake of W30-hCT(9-32) was ~1.4 times higher ($p < 0.02$) than that of unmodified hCT(9-32). However, we attribute the increase in fluorescence upon A23-hCT(9-32) partially to a contribution of incompletely quenched membrane-bound fluorescence. FACS and CLSM data were in good agreement.

Cellular viability of HeLa cells after incubation with the investigated peptides was monitored by an MTT assay. None of the investigated peptides exerted a relevant impact on cellular viability at concentrations ranging from 5 μM to 100 μM (data not shown).

DISCUSSION

The objective of this study was to understand the molecular mechanism of hCT-derived cell-penetrating peptides as related to their association with membrane lipids and the translocation of the plasma membrane. To establish the role of individual residues we investigated hCT(9-32) (19,20) and two mutants thereof. Exchange of residues was performed to enhance the peptides' affinity toward membrane lipids to promote their cellular uptake. For this aim we utilized various experimental techniques from partitioning and leakage experiments to high-resolution NMR spectroscopy to probe peptide-lipid interactions. Biological membranes were mimicked by phospholipid liposomes for partitioning studies and micelles for NMR analysis, respectively. Moreover, we studied the peptides' uptake in HeLa cells.

The mode of interaction of CPPs with the lipid membrane has been vividly discussed. For reviews on this topic see Lundberg et al. (52) and Magzoub et al. (69). To summarize, five different models have been developed: In the case of the inverted micelle model, CPPs associate with the bilayer surface, mainly through electrostatic interactions (53) (Fig. 6 *A*), resulting in containment of the cargo in an inverted micelle and leakage of its contents into the cytosole. In the endocytic mechanism, invaginations in the membrane are formed (Fig. 6 *B*) which later on evolve into vesicles that separate into the cytosole. In the barrel-stave model (Fig. 6 *C*), rearrangements of lipid-associated peptides lead to pore formation. Pores are created by circular assembly of amphipathic peptides in transmembrane fashion in such a way that their hydrophobic domains point to the lipid chains of the membrane and the hydrophilic side chains to the interior of the pore (56). In contrast, in the toroidal model (57) pores are also formed, but headgroups form contacts to transmembrane-inserted peptides throughout (see Fig. 6 *D*).

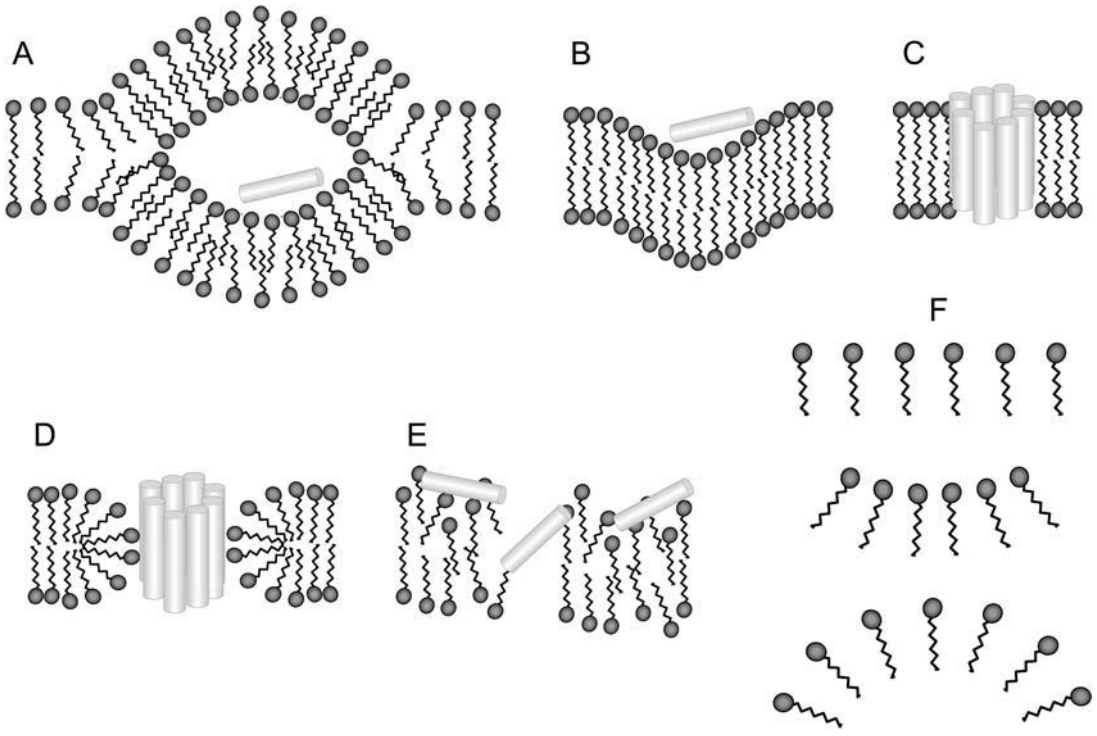

FIGURE 6 Scheme presenting the peptide-phospholipid arrangements in the inverted micelle (*A*), the initial state of the endocytic process (*B*), the barrel-stave (*C*), toroidal pore (*D*), and the carpet mechanism (*E*). The membrane curvature induced by decreased (*F*, *middle*) or increased (*F*, *bottom*) headgroup-headgroup distances are compared to a planar arrangement (*F*, *top*). Note that for clarity, only the outer leaflet is depicted for *F*.

The carpet model (Fig. 6 *E*), on the other hand, which has been previously suggested for the cellular translocation of antimicrobial peptides, assumes an initial association of the peptides with the surface of the membrane. Interactions with basic residues then result in the reorganization of the lipids and cause disruption of lipid packing (54,55). It is believed that the mode of action for CPPs in general may follow different mechanisms.

Which mechanism would apply to a particular CPP will depend on molecular features. In all models described above, an initial association of the peptide with the surface of the bilayer constitutes the first step. Although this step is generally assumed to be governed by electrostatic interactions with negatively charged membrane lipids, hydrophobic partitioning cannot be excluded. The thermodynamics of peptide-lipid interactions has been recently reviewed, and the interested reader is referred to the excellent review by Seelig (58). To which extent electrostatic interactions dominate the first step depends on the presence of basic and acidic amino acids, pH, and salt concentration. Since electrostatic interactions are long range, intrinsic structuring of the peptide is less important for electrostatic association with the membrane as compared to a situation where hydrophobic interactions would dominate. In fact, many membrane-active peptides are unstructured in solution but readily fold in vicinity to the membrane by a coupled partitioning-folding mechanism (59).

Whereas the first step is similar in the three models described above, the following events are different. In the inverted micelle/endocytic models, the peptide remains surface bound throughout the complete translocation process and never penetrates deeply into the hydrophobic interior. In contrast, in the barrel-stave or toroidal pore models the peptide inserts into the membrane in a transmembrane fashion. Whereas no major membrane reorganization occurs in the barrel-stave model, the toroidal pore model implies a rearrangement of phospholipid headgroups such that they interact with the hydrophobic side of the peptide and thereby become transferred into the interior of the membrane. Clearly, pore formation requires an additional interaction interface in the peptide for homo-oligomerization of the CPPs to assemble to the barrel. It is presently not clear which molecular features favor one mechanism over the other. However, it can be expected that balancing and positioning of hydrophobic and hydrophilic residues influence the mechanism. Both properties will have an influence on membrane binding and membrane insertion.

In the barrel-stave model, interactions with the phospholipid headgroups are made by both C- and N-terminal residues. In particular Tyr and Trp residues possess a high tendency to partition into the interface. In the transmembrane segments of helical peptides that favor the barrel-stave mechanism, hydrophobic residues need to be directed toward the outside of the barrel, whereas the inside of the barrel is likely to accommodate hydrophilic residues. Otherwise no pores but helical bundles would be formed. Therefore, the successful assembly of such barrels depends critically on how likely oligomerization is and is also strongly favored in the absence of residues like Tyr and Trp in the central segment of the peptide.

In contrast, in the toroidal pore model, reorganization of the phospholipids occurs such that interactions with phospholipid headgroups take place throughout the helix. Therefore, we expect this mode to be favored when aromatic residues are placed in the central segment and when oligomerization is favored additionally.

The requirements for an inverted-micelle/endocytic type mechanism seem to be different in that a few residues that anchor the peptide on the membrane are sufficient, but their position is probably not critical. In contrast to the toroidal pore mechanism, there is no need for oligomerization. Moreover, the membrane surface in the inverted-micelle mechanism is concave, whereas it is convex in the toroidal pore mechanism (60). A concave membrane surface is formed when the headgroups move together more closely, whereas the convex surface is characterized by increased distances between them (see Fig. 6 *F*). It has been argued that the distance between the headgroups is promoted by electrostatic repulsion. Thus cationic residues may act by partially compensating the negative charges, thereby allowing the headgroups to move more closely together (61). In contrast, intercalation of side chains into the hydrophobic interior may increase distances between headgroups, thereby promoting concave surfaces.

The topology of peptide-lipid aggregates in the carpet model is much less well defined and hence it is more difficult to predict which molecular properties would favor such a mechanism.

The overall hydrophobicity of the peptides and their affinity toward membranes was probed by liposome-buffer partitioning experiments and demonstrated marked to high affinities of hCT-derived peptides to neutral POPC bilayers. In particular, we observed close agreement of partitioning with published thermodynamic data. Wimley and White have experimentally determined free energies of transferring whole amino acids from bulk solution into the membrane-water interface or into the hydrophobic interior (50). The corresponding values for Gly and Trp residues are 0.01 and -1.85 kcal/mol for the transfer into the interface (ΔG_{wif}) and 1.15 and –2.09 kcal/mol into the hydrophobic interior (ΔG_{oct}), respectively. Accordingly, we observed a substantial increase in affinity to POPC LUVs in our partitioning experiments when Gly was replaced by Trp. A similar increase in affinity was observed by replacing Pro^{23} ($\Delta G_{wif} = 0.45$ kcal/mol, $\Delta G_{oct} = 0.14$ kcal/mol) in the middle of the peptide sequence by an Ala ($\Delta G_{wif} = 0.17$ kcal/mol, $\Delta G_{oct} = 0.50$ kcal/mol).

After initial membrane association of the peptides, which is most probably governed by the net charge of the peptide in vicinity to the membrane (note that this may substantially

differ from that in bulk solution), any further steps, in particular those requiring interactions with the hydrophobic side chains, will certainly depend on the structure of the peptides when bound to the membrane. This view is supported by our observation that the partition coefficient of the random sequence is much lower when compared to the values from the hCT-derived peptides demonstrating that, in addition to amino acid sequence, secondary structure also plays a significant role for their affinity to phospholipid membranes. We would like to add that, due to the coupled partitioning-folding mechanism, residues such as Trp are likely to increase membrane-binding affinity and exert a stabilizing effect on secondary structure.

Previously, structures and positioning of the CPPs penetratin and transportan have been determined by NMR in different membrane model systems. Penetratin was found to adopt an α-helical conformation in SDS micelles as well as in partially negatively charged bicelles (62–64), with the helix being parallel aligned to the bicelle surface. Berlose et al. similarly proposed a parallel adoption to the surface also for SDS micelles (62), whereas others could not unambiguously position the peptide on SDS micelles (63). Transportan, a chimeric peptide constructed from galanin and mastoparan, was found to be α-helical in the mastoparan part and mainly unstructured in the galanin part in SDS. Based on spin label experiments, the mastoparan segment inserts into the micelle, whereas the galanin part resides in the interface (65). In a recent study in neutral bicelles, the mastoparan part was observed to adopt a well-defined α-helix, and the galanin part displayed a weaker tendency to form an α-helix. The whole peptide was found to be oriented in parallel with the membrane-water interface (66). Interestingly, like the hCT-derived CPPs investigated in this study, these two peptides were also mainly located at the interface, indicating that an initial strong interaction of the CPPs with membranes is an important prerequisite for translocation.

Structures of the hCT(9-32) peptides in their micelle-bound form are predominantly helical, in contrast to the unligated peptides in solution that are unstructured. hCT (9-32) is characterized by two short helical stretches, extending from Thr^{10} to Asn^{17} and from Gln^{24} to Val^{29}, which, however, possess some additional flexibility. To gain further insight into the importance of secondary structure for translocation, we replaced Pro^{23}, the strongest α-helix breaker, by Ala, which is known to be one of the most efficient α-helix promoters (67). In fact, A23-hCT(9-32) adopted a continuous α-helical structure from residue 12 to 26. Our spin label studies with 5-doxylstearate demonstrated that the more hydrophobic residues Tyr^{12}, Phe^{16}, 18 and 22, and His^{20}, Ala^{23}, and Gly^{28} are integrated into the micelle, leaving the hydrophilic residues Gln^{14} and 24, Asp^{15}, Asn^{17}, and Lys^{18} exposed to the aqueous phase. Thereby A23-hCT(9-32) forms a continuous amphipathic helix. The spin label data for A23-hCT(9-32) nicely reflect periodicity of the helix, also indicating that the peptide was well anchored on the micelle surface. The prolonged helix should result in a larger membrane-binding interface, and this expectation was well met by both the increased partition coefficient as well as the increased propensity for aggregation of fluorescein-labeled A23-hCT(9-32). Unfortunately, the increase in fluorescence intensity as detected by FACS analysis may also be due to formation of aggregates on the cells surface, which would present a drawback for the applicability of A23-hCT(9-32) as a CPP.

In addition, we introduced a Trp residue into the C-terminal segment by replacing Gly^{30}, which in wild-type hCT(9-32) was not associated to the membrane. The $Gly^{30}Trp$ exchange resulted in stable anchoring of the C-terminal segment on the phospholipid micelles, clearly evident from the large attenuations observed in the spin label experiments. The additional membrane-anchor resulted in a twofold increase of the partition coefficient. Interestingly, tighter binding to model membranes in vitro was accompanied by higher uptake into HeLa cells in vitro. The regular, punctuated fluorescence pattern indicated vesicular localization of W30-hCT(9-32) and therefore an endocytic pathway of internalization. The brighter fluorescence of W30-hCT(9-32) as compared to hCT(9-32) observed in the CLSM was confirmed by significantly higher fluorescence detected by FACS analysis. Together with the apparent lack of toxicity, this makes W30-hCT(9-32) a promising CPP candidate for further exploration.

In accordance with our observation of a decreased affinity toward liposomes, a previous study showed that hCT(random) was not taken up into MDCK cells, whereas hCT(9-32) was efficiently internalized (19).

Any mechanism for translocation resulting in membrane permeabilization would be unacceptable from a pharmaceutical point of view when associated with increased cytotoxicity. This study was also performed to reveal whether the CPPs confer cytotoxic effects that would prevent their use in drug delivery. Dye leakage experiments were performed to assure that the sequence modifications do not increase the potential for membrane permeabilization. In fact, no leakage was found to occur for any of the modifications up to a concentration of 50 μM, which was above the concentration used in cell culture experiments (40 μM). At concentrations higher than 50 μM the modified peptides, A23-hCT(9-32) and W30-hCT(9-32), display a slightly increased propensity for leakage relative to hCT(9-32), but remain significantly below the values measured for full-length hCT. Accordingly, in vitro experiments with 5 μM–100 μM peptide solution revealed no effects on cellular viability on HeLa cells, neither for hCT(9-32), nor the modified peptides A23-hCT(9-32) and W30-hCT(9-32). This is in agreement with a previous study where 40 μM hCT(9-32) on MDCK monolayers revealed no significant toxicity after 120 min (19). In addition fluorescein-labeled hCT(9-32) was tested on three different cell lines, and no indications for toxicity were observed for any of the cell lines even at 100 μM, the highest

tested concentration (20). As shown by Christiaens et al. (17), peptides are generally more likely to induce leakage of dye-loaded LUVs than exhibit toxic effects on cell cultures. Nevertheless, in black lipid membranes composed of POPC/DOPG (85:15), untruncated hCT was shown to induce a slight formation of voltage-dependent channels that allow permeation of calcium ions (68) after 200 min of incubation. At the conditions of our study, pore formation as a possible mechanism of translocation can be ruled out. Hence we exclude the cellular translocation of the investigated CPP to follow the barrel-stave model.

Instead, both the spectroscopic part of our work as well as the in vitro studies indicate an endocytic mechanism. The liposome-leakage study disfavors any model that requires permeabilization such as the barrel-stave, the toroidal pore or, to a lesser extent, the carpet model. The structures of hCT(9-32) displayed two rather short helical segments disrupted by Pro^{23}. Replacement of the latter by Ala resulted in a continuous helix. However, spin label data indicated that membrane binding in the central segment was not particularly pronounced as supported by the absence of residues like Trp or Tyr in that segment which would strongly partition into the interface. Rather, the amino acid composition of the peptides implies a moderate association of the peptides with the membrane, and the spin label data indicate that the peptides remain surface associated. Moreover, we see no indication for oligomerization of the peptides in or on the membrane. The initial steps of the inverted micelle model require invaginations of the membrane and are highly similar to early events in endocytosis. Indeed, the punctuated fluorescence pattern indicating vesicular localization of fluorescein-labeled W30-hCT(9-32) suggests that endocytosis takes place, certainly to a considerable extent.

This work was supported by the Commission of the European Union (EU project on Quality of Life and Management of Living Resources, project No. QLK2-CT-2001-01451).

REFERENCES

1. Simeoni, F., M. C. Morris, F. Heitz, and G. Divita. 2003. Insight into the mechanism of the peptide-based gene delivery system MPG: implications for delivery of siRNA into mammalian cells. *Nucleic Acids Res.* 31:2717–2724.
2. Morris, M. C., P. Vidal, L. Chaloin, F. Heitz, and G. Divita. 1997. A new peptide vector for efficient delivery of oligonucleotides into mammalian cells. *Nucleic Acids Res.* 25:2730–2736.
3. Morris, M. C., J. Depollier, J. Mery, F. Heitz, and G. Divita. 2001. A peptide carrier for the delivery of biologically active proteins into mammalian cells. *Nat. Biotechnol.* 19:1173–1176.
4. Lindgren, M., M. Hallbrink, A. Prochiantz, and U. Langel. 2000. Cell-penetrating peptides. *Trends Pharmacol. Sci.* 21:99–103.
5. Derossi, D., G. Chassaing, and A. Prochiantz. 1998. Trojan peptides: the penetratin system for intracellular delivery. *Trends Cell Biol.* 8:84–87.
6. Snyder, E. L., and S. F. Dowdy. 2004. Cell penetrating peptides in drug delivery. *Pharm. Res.* 21:389–393.
7. Schwarze, S. R., K. A. Hruska, and S. F. Dowdy. 2000. Protein transduction: unrestricted delivery into all cells? *Trends Cell Biol.* 10: 290–295.
8. Thoren, P. E., D. Persson, M. Karlsson, and B. Norden. 2000. The Antennapedia peptide penetratin translocates across lipid bilayers—the first direct observation. *FEBS Lett.* 482:265–268.
9. Prochiantz, A. 1996. Getting hydrophilic compounds into cells: lessons from homeopeptides. *Curr. Opin. Neurobiol.* 6:629–634.
10. Lundberg, M., S. Wikstrom, and M. Johansson. 2003. Cell surface adherence and endocytosis of protein transduction domains. *Mol. Ther.* 8:143–150.
11. Wadia, J. S., R. V. Stan, and S. F. Dowdy. 2004. Transducible TAT-HA fusogenic peptide enhances escape of TAT-fusion proteins after lipid raft macropinocytosis. *Nat. Med.* 10:310–315.
12. Vives, E., J. P. Richard, C. Rispal, and B. Lebleu. 2003. TAT peptide internalization: seeking the mechanism of entry. *Curr. Protein Pept. Sci.* 4:125–132.
13. Richard, J. P., K. Melikov, E. Vives, C. Ramos, B. Verbeure, M. J. Gait, L. V. Chernomordik, and B. Lebleu. 2003. Cell-penetrating peptides. A reevaluation of the mechanism of cellular uptake. *J. Biol. Chem.* 278:585–590.
14. Trehin, R., and H. P. Merkle. 2004. Chances and pitfalls of cell penetrating peptides for cellular drug delivery. *Eur. J. Pharm. Biopharm.* 58:209–223.
15. Scheller, A., J. Oehlke, B. Wiesner, M. Dathe, E. Krause, M. Beyermann, M. Melzig, and M. Bienert. 1999. Structural requirements for cellular uptake of alpha-helical amphipathic peptides. *J. Pept. Sci.* 5:185–194.
16. Drin, G., M. Mazel, P. Clair, D. Mathieu, M. Kaczorek, and J. Temsamani. 2001. Physico-chemical requirements for cellular uptake of pAntp peptide. Role of lipid-binding affinity. *Eur. J. Biochem.* 268:1304–1314.
17. Christiaens, B., J. Grooten, M. Reusens, A. Joliot, M. Goethals, J. Vandekerckhove, A. Prochiantz, and M. Rosseneu. 2004. Membrane interaction and cellular internalization of penetratin peptides. *Eur. J. Biochem.* 271:1187–1197.
18. Silverman, S. L. 2003. Calcitonin. *Endocrinol. Metab. Clin. North Am.* 32:273–284.
19. Trehin, R., U. Krauss, R. Muff, M. Meinecke, A. G. Beck-Sickinger, and H. P. Merkle. 2004. Cellular internalization of human calcitonin derived peptides in MDCK monolayers: a comparative study with Tat(47–57) and penetratin(43–58). *Pharm. Res.* 21:33–42.
20. Trehin, R., U. Krauss, A. G. Beck-Sickinger, H. P. Merkle, and H. M. Nielsen. 2004. Cellular uptake but low permeation of human calcitonin-derived cell penetrating peptides and Tat(47–57) through well-differentiated epithelial models. *Pharm. Res.* 21:1248–1256.
21. Trehin, R., H. M. Nielsen, H. G. Jahnke, U. Krauss, A. G. Beck-Sickinger, and H. P. Merkle. 2004. Metabolic cleavage of cell penetrating peptides in contact with epithelial models: human calcitonin (hCT) derived peptides, Tat(47–57) and Penetratin(43–58). *Biochem. J.* 382:945–956.
22. Motta, A., G. Andreotti, P. Amodeo, G. Strazzullo, and M. A. Castiglione Morelli. 1998. Solution structure of human calcitonin in membrane-mimetic environment: the role of the amphipathic helix. *Proteins.* 32:314–323.
23. Wagner, K., A. G. Beck-Sickinger, and D. Huster. 2004. Structural investigations of a human calcitonin-derived carrier peptide in a membrane environment by solid-state NMR. *Biochemistry.* 43:12459–12468.
24. Krauss, U., F. Kratz, and A. G. Beck-Sickinger. 2003. Novel daunorubicin-carrier peptide conjugates derived from human calcitonin segments. *J. Mol. Recognit.* 16:280–287.
25. Pauletti, G. M., and H. Wunderli-Allenspach. 1994. Partition coefficients in vitro: artificial membranes as a standardized distribution model. *Eur. J. Pharm. Sci.* 1:273–282.
26. Buck, R. H., and F. Maxl. 1990. A validated HPLC assay for salmon calcitonin analysis. Comparison of HPLC and biological assay. *J. Pharm. Biomed. Anal.* 8:761–769.
27. Schurtenberger, P., N. Mazer, and W. Kanzig. 1985. Micelle to vesicle transition in aqueous-solutions of bile-salt and lecithin. *J. Phys. Chem.* 89:1042–1049.
28. Mayer, L. D., M. J. Hope, and P. R. Cullis. 1986. Vesicles of variable sizes produced by a rapid extrusion procedure. *Biochim. Biophys. Acta.* 858:161–168.

29. New, R. B. C. 1990. Characterization of liposomes. *In* Liposomes, A Practical Approach. R. B. C. New, editor. Oxford University Press, New York. 125–127.
30. Dathe, M., M. Schumann, T. Wieprecht, A. Winkler, M. Beyermann, E. Krause, K. Matsuzaki, O. Murase, and M. Bienert. 1996. Peptide helicity and membrane surface charge modulate the balance of electrostatic and hydrophobic interactions with lipid bilayers and biological membranes. *Biochemistry.* 35:12612–12622.
31. Brown, L. R., C. Bösch, and K. Wüthrich. 1981. Location and orientation relative to the micelle surface for glucagon in mixed micelles with dodecylphosphocholine: EPR and NMR studies. *Biochim. Biophys. Acta.* 642:296–312.
32. Griesinger, C., G. Otting, K. Wüthrich, and R. R. Ernst. 1988. Clean TOCSY for ^{1}H spin system identification in macromolecules. *J. Am. Chem. Soc.* 110:7870–7872.
33. Kumar, A., R. R. Ernst, and K. Wüthrich. 1980. A two-dimensional nuclear Overhauser enhancement (2D NOE) experiment for the elucidation of complete proton-proton cross-relaxation networks in biological macromolecules. *Biochem. Biophys. Res. Commun.* 95:1–6.
34. Wüthrich, K. 1986. NMR of Proteins and Nucleic Acids. Wiley, New York.
35. Güntert, P., C. Mumenthaler, and K. Wüthrich. 1997. Torsion angle dynamics for NMR structure calculation with the new program DYANA. *J. Mol. Biol.* 273:283–298.
36. Jarvet, J., J. Zdunek, P. Damberg, and A. Gräslund. 1997. Three-dimensional structure and position of porcine motilin in sodium dodecyl sulfate micelles determined by ^{1}H NMR. *Biochemistry.* 36: 8153–8163.
37. Papavoine, C. H., R. N. Konings, C. W. Hilbers, and F. J. Van de Veen. 1994. Location of the M13 major coat protein in sodium dodecylsulfate micelles as determined by NMR. *Biochemistry.* 33: 12990–12997.
38. Bartels, C., T. H. Xia, M. Billeter, P. Güntert, and K. Wüthrich. 1995. The program XEASY for computer-supported spectral analysis of biological macromolecules. *J. Biomol. NMR.* 6:1–10.
39. Bader, R., M. Lerch, and O. Zerbe. 2002. NMR of membrane-associated peptides and proteins. *In* BioNMR in Drug Research. O. Zerbe, editor. Wiley-VCH, Weinheim. 95–120.
40. Bader, R., A. Bettio, A. G. Beck-Sickinger, and O. Zerbe. 2001. Structure and dynamics of micelle-bound neuropeptide Y: comparison with unligated NPY and implications for receptor selection. *J. Mol. Biol.* 305:307–329.
41. Herbig, M. E., U. Fromm, J. Leuenberger, U. Krauss, A. G. Beck-Sickinger, and H. P. Merkle. 2005. Bilayer interaction and localization of cell penetrating peptides with model membranes: a comparative study of a human calcitonin (hCT)-derived peptide with pVEC and pAntp(43–58). *Biochim. Biophys. Acta.* 1712:197–211.
42. Schmidt, M. C., B. Rothen-Rutishauser, B. Rist, A. Beck-Sickinger, H. Wunderli-Allenspach, W. Rubas, W. Sadee, and H. P. Merkle. 1998. Translocation of human calcitonin in respiratory nasal epithelium is associated with self-assembly in lipid membrane. *Biochemistry.* 37: 16582–16590.
43. Wan, C. P., C. S. Park, and B. H. S. Lau. 1993. A rapid and simple microfluorometric phagocytosis assay. *J. Immunol. Methods.* 162:1–7.
44. Sahlin, S., J. Hed, and I. Rundquist. 1983. Differentiation between attached and ingested immune-complexes by a fluorescence quenching cytofluorometric assay. *J. Immunol. Methods.* 60:115–124.
45. Ma, Z. S., and L. Y. Lim. 2003. Uptake of chitosan and associated insulin in Caco-2 cell monolayers: a comparison between chitosan molecules and chitosan nanoparticles. *Pharm. Res.* 20:1812–1819.
46. Tseng, W. C., N. B. Purvis, F. R. Haselton, and T. D. Giorgio. 1996. Cationic liposomal delivery of plasmid to endothelial cells measured by quantitative flow cytometry. *Biotechnol. Bioeng.* 50:548–554.
47. Hed, J., G. Hallden, S. G. Johansson, and P. Larsson. 1987. The use of fluorescence quenching in flow cytofluorometry to measure the attachment and ingestion phases in phagocytosis in peripheral blood without prior cell separation. *J. Immunol. Methods.* 101:119–125.
48. Innes, N. P., and G. R. Ogden. 1999. A technique for the study of endocytosis in human oral epithelial cells. *Arch. Oral Biol.* 44:519–523.
49. Lobner, D. 2000. Comparison of the LDH and MTT assays for quantifying cell death: validity for neuronal apoptosis? *J. Neurosci. Methods.* 96:147–152.
50. White, S. H., and W. C. Wimley. 1998. Hydrophobic interactions of peptides with membrane interfaces. *Biochim. Biophys. Acta.* 1376:339–352.
51. Matsuzaki, K., S. Yoneyama, and K. Miyajima. 1997. Pore formation and translocation of melittin. *Biophys. J.* 73:831–838.
52. Lundberg, P., and U. Langel. 2003. A brief introduction to cell-penetrating peptides. *J. Mol. Recognit.* 16:227–233.
53. Derossi, D., S. Calvet, A. Trembleau, A. Brunissen, G. Chassaing, and A. Prochiantz. 1996. Cell internalization of the third helix of the Antennapedia homeodomain is receptor-independent. *J. Biol. Chem.* 271:18188–18193.
54. Pouny, Y., D. Rapaport, A. Mor, P. Nicolas, and Y. Shai. 1992. Interaction of antimicrobial dermaseptin and its fluorescently labeled analogues with phospholipid membranes. *Biochemistry.* 31:12416–12423.
55. Matsuzaki, K., K. Sugishita, and K. Miyajima. 1999. Interactions of an antimicrobial peptide, magainin 2, with lipopolysaccharide-containing liposomes as a model for outer membranes of gram-negative bacteria. *FEBS Lett.* 449:221–224.
56. Gazit, E., W. J. Lee, P. T. Brey, and Y. Shai. 1994. Mode of action of the antibacterial cecropin B2: a spectrofluorometric study. *Biochemistry.* 33:10681–10692.
57. Matsuzaki, K., O. Murase, N. Fujii, and K. Miyajima. 1996. An antimicrobial peptide, magainin 2, induced rapid flip-flop of phospholipids coupled with pore formation and peptide translocation. *Biochemistry.* 35:11361–11368.
58. Seelig, J. 2004. Thermodynamics of lipid-peptide interactions. *Biochim. Biophys. Acta.* 1666:40–50.
59. Popot, J. L., and D. M. Engelman. 2000. Helical membrane protein folding, stability, and evolution. *Annu. Rev. Biochem.* 69:881–922.
60. Lundberg, P., and U. Langel. 2003. A brief introduction to cell-penetrating peptides. *J. Mol. Recognit.* 16:227–233.
61. Kirk, G. L., S. M. Gruner, and D. L. Stein. 1984. A thermodynamic model of the lamellar to inverse hexangonal phase transition of lipid-membrane water systems. *Biochemistry.* 23:1093–1102.
62. Berlose, J. P., O. Convert, D. Derossi, A. Brunissen, and G. Chassaing. 1996. Conformational and associative behaviours of the third helix of Antennapedia homeodomain in membrane-mimetic environments. *Eur. J. Biochem.* 242:372–386.
63. Lindberg, M., H. Biverstahl, A. Gräslund, and L. Mäler. 2003. Structure and positioning comparison of two variants of penetratin in two different membrane mimicking systems by NMR. *Eur. J. Biochem.* 270:3055–3063.
64. Lindberg, M., and A. Gräslund. 2001. The position of the cell penetrating peptide penetratin in SDS micelles determined by NMR. *FEBS Lett.* 497:39–44.
65. Lindberg, M., J. Jarvet, U. Langel, and A. Gräslund. 2001. Secondary structure and position of the cell-penetrating peptide transportan in SDS micelles as determined by NMR. *Biochemistry.* 40:3141–3149.
66. Barany-Wallje, E., A. Andersson, A. Gräslund, and L. Mäler. 2004. NMR solution structure and position of transportan in neutral phospholipid bicelles. *FEBS Lett.* 567:265–269.
67. Chou, P. Y., and G. D. Fasman. 1977. Secondary structural prediction of proteins from their amino-acid sequence. *Trends Biochem. Sci.* 2:128–131.
68. Stipani, V., E. Gallucci, S. Micelli, V. Picciarelli, and R. Benz. 2001. Channel formation by salmon and human calcitonin in black lipid membranes. *Biophys. J.* 81:3332–3338.
69. Magzoub, M., and A. Gräslund. 2004. Cell-penetrating peptides: small from inception to application. *Q. Rev. Biophys.* 37:147–195.